

Mobility Measurements of Immunomagnetically Labeled Cells Allow Quantitation of Secondary Antibody Binding Amplification

Kara E. McCloskey,^{1,2} Kristin Comella,² Jeffrey J. Chalmers,² Shlomo Margel,³ Maciej Zborowski¹

¹Department of Biomedical Engineering/ND-20, The Cleveland Clinic Foundation, 9500 Euclid Avenue, Cleveland Ohio. 44195; telephone: +216 445-9330; fax: +216 444-9198; e-mail: zborow@bme.ri.ccf.org

²Department of Chemical Engineering, The Ohio State University, 140 W. 19th Avenue, Columbus, Ohio 43210; telephone: 614 292-2727; fax: 614 292-3769; e-mail: chalmers.1@osu.edu

³Bar-Ilan University, Department of Chemistry, 52900 Ramat-Gan, Israel

Received 26 December 2000; accepted 25 June 2001

Abstract: Magnetic cell separation methods commonly utilize paramagnetic materials conjugated to antibodies that target specific cell surface molecules. The amount of magnetic material bound to a cell is directly proportional to the magnetophoretic mobility of that cell. A mathematical model has been developed which characterizes the fundamental parameters controlling the amount of magnetic material bound, and thus, the magnetophoretic mobility of an immunomagnetically labeled cell. In characterization of the paramagnetic labeling, one of the parameters of interest is the increase in magnetophoretic mobility due to the secondary antibody binding to multiple epitopes on the primary antibody, referred to as the "secondary antibody binding amplification," Ψ . Secondary antibody-binding amplification has been investigated and quantitated by comparing the mobilities of lymphocytes directly labeled with anti-CD4 MACSTM (Miltenyi Biotec, Auburn, CA) magnetic nanoparticle antibody with the mobilities of lymphocytes from the same sample labeled with two different indirect antibody-labeling schemes. Each indirect labeling scheme incorporated a primary mouse anti-CD4 FITC antibody that provides both FITC and mouse-specific binding sites for two different secondary antibody-magnetic nanoparticle conjugates: either anti-FITC MACS magnetic nanoparticle antibody or anti-mouse MACS magnetic nanoparticle antibody. The magnetophoretic mobilities of the immunomagnetically labeled cells were obtained using Cell Tracking Velocimetry (CTV). The results indicate that an average of 3.4 anti-FITC MACS magnetic nanoparticle antibodies bind to each primary CD4 FITC antibody, $\Psi_{1,2f} = 3.4 \pm 0.33$, and that approximately one, $\Psi_{1,2m} = 0.98 \pm 0.081$, anti-mouse MACS magnetic nanoparticle antibody binds to each primary mouse CD4 FITC antibody on a CD4 positive lymphocyte. These results have provided a better understanding of the antibody-

binding mechanisms used in paramagnetic cell labeling for magnetic cell separation. © 2001 John Wiley & Sons, Inc. *Biotechnol Bioeng* 75: 642–655, 2001.

Keywords: antigen density; quantitative flow cytometry; antibody binding capacity; magnetic cell separation; magnetophoretic mobility; particle tracking velocimetry

INTRODUCTION

The ability to isolate and analyze cells has important applications in fundamental biological studies as well as in the diagnosis and treatment of human diseases. For example, hematopoietic progenitor cells isolated from human umbilical cord blood, normal bone marrow, and peripheral blood are able to reconstitute hematopoiesis in humans and may be used for the treatment of patients having undergone chemotherapy (de Wynter et al., 1995; Handgretinger et al., 1998). Other medical applications for cell separation include the isolation of putative progenitor cells for angiogenesis (Asahara et al., 1997) and separation of cancer cells from blood for analysis and early diagnosis (Racila et al., 1998).

Immunological methods such as immunofluorescent, immunomagnetic, and immunomatrix methods are typically employed to achieve cell separations and analysis based on the expression of specific molecules on or within the cell. Of these methods, immunomagnetic cell separation is the current interest of our laboratories, more specifically, non-batch, high-throughput quadrupole and dipole immunomagnetic cell flow-sorting devices (Moore et al., 1998; Sun et al., 1998). The quadrupole magnetic flow sorter has distinct advantages in that it is able to process a larger numbers of cell more quickly than current batch systems. It is also potentially less expensive and orders of magnitude faster than fluorescent activated cell sorters (FACS). In addition, magnetic

Correspondence to: Maciej Zborowski
Contract grant sponsors: National Science Foundation; National Cancer Institute
Contract grant numbers: BCS-9258004; BES-9731059; ROICA62349; R33 CA81662-01

flow sorting does not induce the high cellular shear stresses that are present in FACS separation.

Immunomagnetic separation processes commonly employ paramagnetic nanoparticles conjugated to antibodies directed against cellular antigens. The use of these paramagnetic nanoparticles, as opposed to paramagnetic microparticles, creates a situation where the volume of magnetic reagent, or degree of immunomagnetic labeling, bound to the targeted cellular molecules is related to the expression level of those targeted molecules. Thus, the volume of magnetic reagent bound to a cell will dictate the cell's mobility when that cell is placed in an external magnetic field gradient. Knowledge of this degree of immunomagnetic labeling is a central consideration in the design and operation of continuous immunomagnetic cell separation (Chalmers et al., 1998, 1999a; Moore et al., 1998, Sun et al., 1998 Williams et al., 1999, Zborowski et al., 1999).

The degree of immunomagnetic labeling is measured using a motion analysis technique to determine the magnetic susceptibility, or magnetophoretic mobility, of an immunomagnetically labeled cell (or particle), on a cell-by-cell-basis (Reddy et al., 1998). This technique, also developed in our laboratories, involves videotaping the movement of immunomagnetically labeled cells through a medium of known viscosity and magnetic susceptibility in a well-defined magnetic energy density gradient. The velocity of each cell along with its location within the magnetic energy gradient is recorded. From this information, the magnetic susceptibility of each cell is calculated. This technique, referred to as Cell Tracking Velocimetry (CTV), includes semiautomated computer video imaging and tracking analysis (Chalmers et al., 1999a, 1999b). A recent advancement in the CTV instrument is in the magnet design, where the magnet now includes a region of nearly constant magnetic energy gradient. Within this specified region, cell mobility is independent of cell position, thus vastly simplifying the data analysis (Chalmers et al., 1999c; Moore et al., 2000).

One of the parameters governing the degree of immunomagnetic labeling and thus, magnetophoretic mobility of an immunomagnetically labeled cell is called the "antibody-binding capacity" or ABC (Zagursky et al., 1995). Antibody binding capacity is a term that provides quantitative information about the number of primary antibodies binding to the targeted surface molecules on individual cells. Just as the fluorescent intensity from a flow cytometer (FCM) is proportional to cellular ABC, it has been shown that, within a specific range, magnetophoretic mobility is directly proportional to ABC (McCloskey et al., 2000).

In previous publications, a mathematical model and methodology, incorporating CTV technology, were presented that describe using paramagnetically labeled calibration microbeads and a genetically modified fibrosarcoma cell line to correlate magnetophoretic mobility to ABC. This correlation was then used to

quantitate the ABC of the cells (McCloskey et al., 2000; 2001). The mathematical model also includes parameters that indicate that the primary and secondary antibody reagents used in the immunomagnetic labeling procedure influence the final magnetophoretic mobility of an immunomagnetically labeled cell or microbead. Our goal here is to show that the secondary antibody-binding amplification factor, due to secondary antibodies binding to multiple binding sites on the primary antibody, is an important parameter in the characterization of magnetophoretic mobility. We also show how one may quantitate secondary antibody-binding amplification by comparing mean magnetophoretic mobilities from three different indirect antibody-labeling schemes with the mean magnetophoretic mobility of cells labeled using a direct antibody-labeling scheme.

MATHEMATICAL MODEL OF MAGNETOPHORESIS

For a paramagnetically labeled cell or microbead, the forces determining its movement through a liquid suspension are magnetic (F_m), buoyancy (F_{bou}), gravity (F_g), and drag (F_d) forces. The magnetic force acting on an immunomagnetically labeled cell or microbead using a two-step labeling protocol has been previously published (McCloskey et al., 2000).

$$F_m = (n_1\theta_1\lambda_1)(n_2\theta_2\lambda_2)n_3F_b \quad (1)$$

F_b is the magnetic force acting on one paramagnetic nanoparticle in the direction of the magnetic energy gradient. Subscripts "1" and "2" refer to the primary and secondary labeling antibodies, respectively; n_1 is the number of antigen-binding sites per cell, including specific and nonspecific antigen sites ($n_s + n_{ns}$) and θ_1 is the fraction of antigen molecules on the particle surface bound by primary antibody. The parameter, λ_1 , represents the valence of the primary antibody binding. For example, it has been shown that one fully intact anti-CD4 (Leu 3a) antibody typically binds two CD4 cellular antigen molecules, exhibiting classical bivalent antibody binding. In this instance, the value for λ_1 is one half (Davis et al., 1998).

The combined term $n_1\theta_1\lambda_1$ is equivalent to the commonly used term "antibody-binding capacity" (ABC) of a cell population (Zagursky et al., 1995). Antibody-binding capacity is a measure of the number of primary antibodies binding to a cell or microbead. This value includes not only the number of antigen molecules per cell, but also variables such as valence of antibody binding, steric hindrance, binding affinities, and non-specific binding. Thus:

$$ABC = n_1\theta_1\lambda_1 \quad (2)$$

The same sequence of parameters is then repeated for the binding of the secondary antibody to sites on the

primary antibody. In this case, n_2 is the number of binding sites on the primary antibody recognized by the secondary antibody. For example, if the secondary antibody is a mouse anti-fluorescein isothiocyanate (FITC), n_2 will be the number of FITC molecules conjugated to that primary antibody. This value is often referred to as the fluorescein-to-protein ratio (F/P) of the antibody reagent (Schwartz and Fernández-Repollet, 1994). θ_2 is the fraction of binding sites on the primary antibodies that are bound by secondary antibodies, and λ_2 represents the valence of the secondary antibody binding (i.e., the number of secondary antibodies that bind per one FITC molecule). These terms $n_2\theta_2\lambda_2$ can then be combined into one overall term, Ψ :

$$\Psi = n_2\theta_2\lambda_2 \quad (3)$$

representing the antibody-binding amplification due to the secondary antibody binding to multiple sites on the primary antibody, or the number of secondary antibodies binding per primary antibody.

The final parameter, n_3 represents the number of magnetic nanoparticles conjugated to the antibody. [Note that due to a publishing error in McCloskey et al. (2000), the value β_2 was used in the formulas instead of n_3]. In magnetic cell-separation applications, it is usually the secondary antibody that is conjugated to the magnetic nanoparticle, so n_3 represents the number of magnetic nanoparticles conjugated to the secondary antibody. In the case where cells are directly labeled, i.e., that there is only one primary antibody, no secondary antibody, and the magnetic particles are conjugated to this primary antibody, then n_3 would represent the number of magnetic nanoparticles conjugated to the primary antibody. Providing that the chemistry of the antibody binding to the magnetic nanoparticle is the same, and that both types of antibody (primary and secondary) magnetic nanoparticle conjugates come from the same manufacturer, the parameter n_3 is the same for the magnetic nanoparticles attached to either the primary or the secondary antibody.

Combining parameters $n_2\theta_2\lambda_2n_3$ into one overall term, β , gives a value that represents the number of magnetic nanoparticles bound to each primary antibody on a cell or microbead. The lumped term βABC describes the number of magnetic nanoparticles bound to each cell or microbead, and is therefore referred to as the “magnetic particle-binding capacity” of a cell or microbead.

The CTV instrument, used to experimentally measure magnetophoretic mobility, is oriented such that the magnetic energy gradient in the experimental system is perpendicular to gravity, thus the governing forces are magnetic forces, F_m , as described in Equation (1), and drag force, F_d , which follows Stokes’ law for slow-moving particles. Setting these two opposing forces equal to

one another (negligible particle inertia), we obtain a relationship for the magnetic energy gradient-induced velocity, v_c , of the magnetized cell or microbead:

$$v_c = \frac{(n_1\theta_1\lambda_1)(n_2\theta_2\lambda_2)n_3\|F_b\|}{3\pi D_c\eta} = \frac{ABC\Psi n_3\|F_b\|}{f} \quad (4)$$

where D_c is the diameter of the cell or microbead, η is the viscosity of the fluid, and $f = 3\pi D_c\eta$ is the friction coefficient of the moving cell or microbead. Dividing the velocity value by the magnetophoretic driving force, S_m , gives us the magnetophoretic mobility, m , a “normalized” parameter analogous to electrophoretic mobility, of the immunomagnetically labeled cell or microbead:

$$m = \frac{v_c}{S_m} = \frac{k}{f} \Psi n_3 ABC \quad (5)$$

where $k = \Delta\chi V_m$ is a constant representing the magnetic property of a single magnetic nanoparticle, $\Delta\chi$ is the difference in magnetic susceptibility between the magnetic material, χ_b , and the surrounding medium, χ_f , and V_m is the volume of paramagnetic material per paramagnetic nanoparticle.

The above equation includes the combined parameters, $\Psi = n_2\theta_2\lambda_2$ which represent the antibody-binding amplification due to the secondary antibody binding to multiple sites on each primary antibody. The work outlined in this article is our investigation into the value of this secondary antibody-binding amplification term. This was accomplished by comparing the magnetophoretic mobilities of two different indirect (two-step) antibody-labeling schemes with the mobility of a direct (single-step) antibody-labeling scheme, all directed against the CD4 antigen on human T-lymphocytes. The magnetic nanoparticles used in this work were MACS™ nanoparticles (dextran ferrite colloids, nominal diameter of 50 nm, purchased from Miltenyi Biotec, Auburn, CA).

METHODS FOR CALCULATING SECONDARY ANTIBODY-BINDING AMPLIFICATION

The first antibody-labeling scheme uses a mouse anti-CD4 FITC primary antibody and a mouse anti-FITC MACS magnetic nanoparticle secondary antibody, Figure 1a. The expression for the magnetophoretic mobility using this first antibody-labeling scheme is as follows:

$$m_{1,2f} = \frac{(n_1\theta_1\lambda_1)(n_2\theta_{2f}\lambda_{2f})n_3k}{f} = \frac{(n_1\theta_1\lambda_1)\Psi_{1,2f}n_3k}{f} \quad (6)$$

where subscript “1” refers to the mouse anti-CD4 FITC primary antibody and subscript “2f” refers to the mouse anti-FITC MACS magnetic nanoparticle secondary antibody. Because the antibody amplification factor, Ψ , depends on the number of sites on the pri-

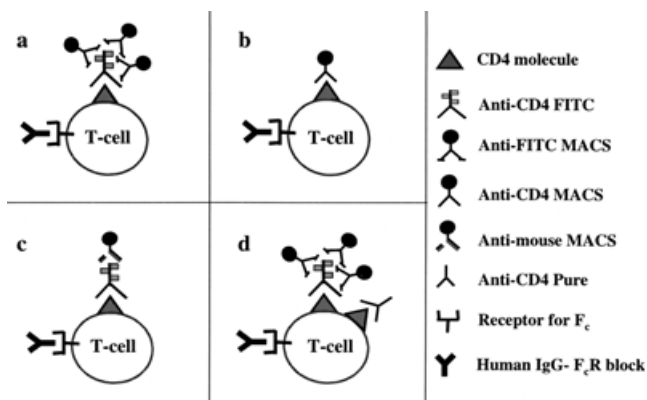


Figure 1. (a) Schematic of CD4 positive lymphocyte cell labeled with an anti-CD4 FITC primary antibody and anti-FITC MACS magnetic nanoparticle antibody (labeling scheme 1). (b) Schematic of CD4 positive lymphocyte cell labeled with an anti-CD4 MACS magnetic nanoparticle antibody (labeling scheme 2). (c) Schematic of CD4 positive lymphocyte cell labeled with a mouse anti-CD4 FITC primary antibody and anti-mouse MACS magnetic nanoparticle antibody (labeling scheme 3). (d) Schematic of CD4 positive lymphocyte cell labeled with FITC conjugated and unconjugated anti-CD4 primary antibodies and anti-FITC MACS magnetic nanoparticle antibody (labeling scheme 4).

mary antibody for the secondary antibody to bind, the subscript includes both “1” and “2f” denoting that this factor is dependent on both the primary and secondary antibodies.

The second antibody-labeling scheme incorporates a direct labeling approach using mouse anti-CD4 MACS magnetic nanoparticles as the only antibody, Figure 1b. The expression for the magnetophoretic mobility using this second antibody-labeling scheme is as follows:

$$m_{1D} = \frac{(n_{1D}\theta_{1D}\lambda_{1D})n_3k}{f} \quad (7)$$

where subscript “1D” refers to the direct (single-step) mouse anti-CD4 MACS magnetic nanoparticle antibody used to label these cells. Here, the mouse anti-CD4 MACS magnetic nanoparticle antibody was carefully chosen so that it was from the same clone (SK3) as the mouse anti-CD4 FITC-conjugated antibody (used in schemes a, b, and d) and the mouse anti-CD4 unconjugated primary antibody (used in scheme d). Because these products use the same antibody, the only differences between them are that they are either unconjugated antibodies, conjugated with FITC molecules, or conjugated with magnetic nanoparticles. Assuming that the conjugation of either FITC molecules or a magnetic nanoparticle to the antibody does not affect the antibody’s specificity, valence, or binding affinity, we set $n_{1D} = n_1$, $\theta_{1D} = \theta_1$, and $\lambda_{1D} = \lambda_1$. Now, the above equation can be rewritten:

$$m_{1D} = \frac{(n_1\theta_1\lambda_1)n_3k}{f} \quad (8)$$

Note that n_3 , the number of magnetic particles conjugated to the antibody, is assumed to be the same

whether or not the antibody is used as a primary or a secondary antibody.

This assumption is valid as long as the magnetic particle-antibody conjugates are purchased from the same vendor. Equations (6) and (8) may now be further manipulated to isolate the secondary antibody binding amplification factor, Ψ . By dividing Equation (6) by Equation (8), one obtains:

$$\frac{m_{1,2f}}{m_{1D}} = \frac{\frac{(n_1\theta_1\lambda_1)\psi_{1,2f}n_3k}{f}}{\frac{(n_1\theta_1\lambda_1)n_3k}{f}} = \Psi_{1,2f} \quad (9)$$

where $\Psi_{1,2f}$ is the antibody-binding amplification factor corresponding to the labeling scheme in Figure 1a.

The third antibody-labeling scheme uses the same primary mouse anti-CD4 FITC antibody as in the first scheme, but uses a different secondary antibody, a rat anti-mouse MACS magnetic nanoparticle antibody, Figure 1c. The mathematical expression for the cellular magnetophoretic mobility produced by the third antibody-labeling scheme follows:

$$m_{1,2m} = \frac{(n_1\theta_1\lambda_1)(n_{2m}\theta_{2m}\lambda_{2m})n_3k}{f} = \frac{(n_1\theta_1\lambda_1)\Psi_{1,2m}n_3k}{f} \quad (10)$$

where subscript “1” refers to the mouse anti-CD4 FITC primary antibody and subscript “2m” refers to the rat anti-mouse MACS magnetic nanoparticle secondary antibody. Again, by dividing Equation (10) by Equation (8), one obtains:

$$\frac{m_{1,2m}}{m_{1D}} = \frac{\frac{(n_1\theta_1\lambda_1)\Psi_{1,2m}n_3k}{f}}{\frac{(n_1\theta_1\lambda_1)n_3k}{f}} = \Psi_{1,2m} \quad (11)$$

where $\Psi_{1,2m}$ is the antibody-binding amplification factor corresponding to the labeling scheme in Figure 1c.

The last antibody-labeling protocol incorporated a mixture of mouse anti-CD4 FITC-conjugated and unconjugated (pure) primary antibodies and anti-FITC MACS magnetic nanoparticle secondary antibodies. This antibody-labeling scheme, depicted in Figure 1d, is similar to the first antibody-labeling scheme in Figure 1a. The difference between these two schemes is the additional amount of unconjugated antibody that was added to compete with the mouse anti-CD4 FITC-conjugated antibodies. We predicted that this would decrease the total number of sites available for the secondary antibody to bind. The expression for the magnetophoretic mobility for this fourth antibody-labeling scheme follows:

$$m_{1,2\phi} = \frac{(n_1\theta_1\lambda_1)(n_{2\phi}\theta_{2\phi}\lambda_{2\phi})n_3k}{f} \quad (12)$$

where subscript “1” refers to the mouse anti-CD4 FITC-conjugated and mouse anti-CD4 unconjugated primary antibodies and subscript “2φ” refers to the

number of binding sites specific for secondary antibody binding given that now only a fraction, ϕ , of FITC sites are available as compared with using the anti-CD4 FITC-conjugated antibody alone. Remembering that n_{2f} has been defined as the number of binding sites on the primary antibody specific for secondary antibody binding and recognizing that the average number of binding sites on the primary antibody for secondary antibody will now be a fraction of the average number of sites available as when using mouse anti-CD4 FITC alone, we see that:

$$n_{2\phi} = \phi n_{2f} \quad (13)$$

By dividing Equation (12) by Equation (6) and substituting in Equation (13), we obtain:

$$\frac{m_{1,2\phi}}{m_{1,2f}} = \frac{\frac{(m_1\theta_1\lambda_1)(n_{2\phi}\theta_2\lambda_2)n_3k}{f}}{\frac{(m_1\theta_1\lambda_1)(n_{2f}\theta_2\lambda_2)n_3k}{f}} = \phi \quad (14)$$

Thus, the decrease in the magnetophoretic mobility due to the addition of the competing antibody is equal to the fraction of the cell molecule antigen sites that are occupied by the FITC-conjugated antibody out of the total number of sites occupied by the two antibodies.

MATERIALS AND METHODS

Cell Preparation

Whole blood from apparently healthy donors was purchased from the American Red Cross, Central Ohio Region (Columbus, OH). A Ficoll-Paque density gradient centrifugation method (Amersham Pharmacia Biotech, Uppsala, Sweden) was used to obtain the peripheral blood mononuclear (PBMN) cell layer. The excess red blood cells were removed using a lysis buffer consisting of 154 mM NH₄CL, 10 mM KHCO₃, and 0.1 mM EDTA for 10 min.

Because monocytes as well as T-lymphocytes, express CD4 molecules the monocytes were removed from the white blood cell population by adhering the monocytes to plastic. The 125 million cells were suspended in 50 mL of RPMI media. Five aliquots of this cell suspension were then poured into T-75 cell culture flasks and incubated for 30 min at 37°C allowing the monocytes to adhere to the surface of the flask. The nonadherent cells were collected and washed with a PBS-buffer solution containing 0.1% BSA and 2 mM EDTA in calcium- and magnesium-free phosphate buffer solution (prepared in-house). Aliquots of approximately 4 million enriched PBMNs were placed in four 15-mL centrifuge tubes along with 500 μ L of buffer solution and 25 μ L of human IgG blocker (Miltenyi Biotec, Auburn, CA). These cells were then immunomagnetically bound by MACS magnetic nanoparticles using the four different antibody-labeling schemes as described below.

Scheme 1: Anti-CD4 FITC Antibodies and Anti-FITC MACS Magnetic Nanoparticles

A saturating amount, 200 μ L (50 μ L per million cells) of primary monoclonal mouse (Isotype IgG1, Clone SK3) anti-CD4 (LeuTM3a) FITC antibodies (Becton Dickinson Immunocytometry Systems, San Jose, CA, Lot # 15114, F/P = 6.55) was added to the tube and incubated for 30 min at 7°C. These cells were then washed once and resuspended in 500 μ L of buffer solution. A saturating amount, 200 μ L (50 μ L per million cells) of secondary monoclonal mouse (Isotype: IgG1) anti-FITC MACS magnetic nanoparticle antibodies (Miltenyi Biotec, Lot # 5000320036) was then added to the tube and incubated for 30 min at 7°C. These cells were then washed twice and resuspended in 2 mL of buffer solution and analyzed by CTV. A diagram of this immunomagnetic labeling scheme is shown in Figure 1a. The saturating amounts of antibody reagents were predetermined as described below.

Scheme 2: Anti-CD4 MACS Magnetic Nanoparticles

Two hundred microliters of primary monoclonal mouse (Isotype IgG1, Clone SK3) anti-CD4 (Leu3a) MACS magnetic nanoparticle antibodies (Miltenyi Biotec, Lot # 5000228005) were added to the tube and incubated for 30 min at 7°C. These cells were then washed twice and resuspended in 2 mL of buffer solution and analyzed by CTV. A diagram of this immunomagnetic labeling scheme is shown in Figure 1b.

Scheme 3: Anti-CD4 FITC Antibodies and Anti-mouse MACS Magnetic Nanoparticles

A saturating amount, 200 μ L, of primary monoclonal mouse (Isotype IgG1, Clone SK3) anti-CD4 (Leu3a) FITC antibodies (Lot # 15114, F/P = 6.55) was added to the tube and incubated for 30 min at 7°C. These cells were then washed once and resuspended in 500 μ L of buffer solution and then 200 μ L of secondary monoclonal rat anti-mouse IgG1 MACS magnetic nanoparticle antibodies (Miltenyi Biotec, Lot # 5990927018) were added to the tube and incubated for 30 min at 7°C. These cells were then washed twice and resuspended in 2 mL of buffer solution and analyzed by CTV. A diagram of this immunomagnetic labeling scheme is shown in Figure 1c.

Scheme 4: A 50:50 v/v Mixture of Anti-CD4 Antibodies (Unconjugated and FITC Conjugated) and Anti-FITC MACS Magnetic Nanoparticles

Primary monoclonal mouse (Isotype IgG1, Clone SK3) anti-CD4 (Leu3a) FITC antibody (Lot # 15114, F/P = 6.55) and primary monoclonal mouse (Isotype IgG1, Clone SK3) anti-CD4 (Leu3a) Pure (Becton Dickinson

Immunocytometry Systems Lot # 11546, F/P = 0) were both added, 100 μL of each antibody reagent, to the tube and incubated for 30 min at 7°C. These cells were then washed once and resuspended in 500 μL of buffer solution. A saturating amount, 200 μL , of secondary monoclonal mouse (Isotype: IgG1) anti-FITC MACS magnetic nanoparticle antibodies (Lot # 5000320036) was then added to the tube and incubated for 30 min at 7°C. These cells were then washed twice and resuspended in 2 mL of buffer solution and analyzed by CTV. A diagram of this immunomagnetic labeling scheme is shown in Figure 1d.

Antibody Saturation Studies

Experiments were conducted to ensure that the concentration of antibody reagent used for cell immunolabeling was sufficient to saturate the available antigen-binding sites. To ensure this, cells from one blood sample, including monocytes, were incubated with different amounts of the anti-CD4 FITC-conjugated antibody reagent following the protocols above. Figure 2a depicts the results from the saturation study for the primary CD4 FITC antibody. Median fluorescence intensities of the CD4 positive lymphocyte cell population

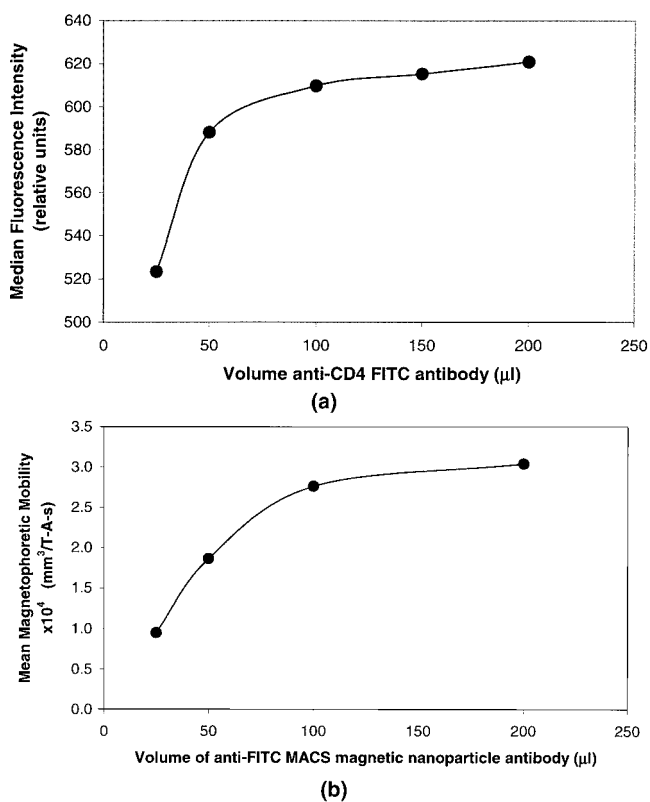


Figure 2. (a) Cellular fluorescence intensity as a function of the added primary anti-CD4 FITC antibody. (b) Cellular magnetophoretic mobility as a function of the added secondary anti-FITC MACS magnetic nanoparticle antibody.

from FCM analysis (FACScan, Becton Dickinson Immunocytometry Systems) are plotted vs. the volume of CD4 FITC antibody reagent used for 2 million total cells suspended in 250 μL of PBS-buffer solution and 25 μL of human IgG blocker. The 2 million total cells exhibit saturation at 100 μL of antibody reagent.

A separate blood sample was used for the secondary saturation study for the anti-FITC MACS magnetic nanoparticle-conjugated antibody. For this study, amounts and volumes described above were scaled-up by a factor of two to accommodate for the larger cell numbers needed for CTV analysis as compared with FCM analysis. Figure 2b depicts the mean magnetophoretic mobilities of the CD4 positive lymphocyte cell population from CTV analysis plotted vs. the volume of anti-FITC MACS magnetic nanoparticle antibody reagent used for 4 million total cells suspended in 500 μL of PBS-buffer solution and 25 μL of human IgG blocker. The optimized amounts, 200 μL of primary CD4 FITC antibody and 200 μL of secondary MACS magnetic nanoparticle antibody per 4 million total cells suspended in 500 μL of PBS-buffer solution and 25 μL of human IgG blocker, were then used for labeling with all reagents in the protocols above.

Immunofluorescent Labeling of Quantum Simply Cellular[®] Microbeads

Quantum Simply Cellular (QSC) calibration microbeads were analyzed using FCM to check the accuracy of the results from scheme 4 (Figure 1d) in which the anti-CD4 FITC-conjugated primary antibodies were mixed with unconjugated anti-CD4 antibodies. Quantum Simply Cellular[®] microbeads (Flow Cytometry Standards Corporation, San Juan, PR) are polystyrene microbeads of 8 microns in diameter. The microbeads have calibrated numbers of goat anti-mouse antibodies (GAM) bound to their surfaces. Individual sets of these microbeads are coated with four distinct populations of GAM antibodies that bind the Fc region of IgG1, IgG2a, and IgG2b isotypes of mouse monoclonal antibodies and one blank microbead population for controls. The median ABC values for the population sets are 0, 5,600, 18,000, 51,000, and 150,000.

Aliquots of 100 μL of the QSC microbeads at concentration of 2 million per mL were placed in two different 15-mL centrifuge tubes along with 100 μL of PBS. A saturating amount, 100 μL , of monoclonal mouse (Isotype IgG1, Clone SK3) anti-CD4 (Leu3a) FITC antibodies (Becton Dickinson Immunocytometry Systems, Lot # 15114, F/P = 6.55) was added to one tube and 50 μL of the same monoclonal mouse anti-CD4 (LeuTM3a) FITC antibody along with 50 μL of monoclonal mouse (Isotype IgG1, Clone SK3) anti-CD4 (Leu3a) Pure (Lot # 11546) were both added to the second tube and incubated for 1 h at room temperature. These microbeads were then washed twice with 2 mL of

PBS and resuspended in 300 μ L of PBS, now ready for FCM analysis.

Cell Concentration Effects on Mobility

In CTV analysis, we make the assumption that there are no cell-cell interactions. If correct, the magnetophoretic mobility of each cell would be independent of the surrounding cells. To test for possible evidence of interparticle interactions, studies have been conducted which measure the concentration effects of monodisperse (diameter = 2.7 microns) magnetite/maghemite-coated polymeric microspheres with nonmagnetic microspheres (microspheres without any magnetite coating). A complete description and evaluation of these magnetic microspheres has been previously published (Margel et al., 1997; Moore et al., 2000).

Four separate microsphere samples were prepared for CTV analysis. The first sample contained a homogeneous population of the nonmagnetic microspheres suspended in PBS. The second sample contained a homogeneous population of the magnetite/maghemite-coated magnetic microspheres suspended in PBS. The third sample contained 1 million nonmagnetic microspheres mixed with 1 million magnetite-coated microspheres, all suspended in 1 mL of PBS producing a final concentration of 2 million microspheres per mL of PBS. The fourth sample contained 250 thousand nonmagnetic microspheres mixed with 250 thousand magnetite-doped microspheres, all suspended in 1 mL of PBS producing a final concentration of 0.5 million microspheres per mL of PBS. The magnetophoretic mobilities of each of these samples were measured by CTV analysis.

The CTV Apparatus

The CTV image analysis system was designed to measure the velocity of the paramagnetically labeled cells or other similar-sized particles in a well-defined magnetic energy gradient. The microbead sample was pumped with a Harvard PhD 2000 Programmable Syringe Pump (Holliston, MA), fitted with a 1-cc syringe, in the z-direction, perpendicular to gravity (x-direction), through flexible tubing into a 1-mm ID square glass channel. An inverted microscope with a 5 \times objective was focused on the microbeads in the glass channel at the appropriate region of constant force (along the y-direction). Light was supplied to the microscope by a Fiber Lite (Dolan-Jenner, Lawrence, MA) fiber optic light source with a fiber optic cable. The movement of the cells or microbeads in the magnetic energy gradient (along the z-direction) was videotaped with a 30 Hz Cohu (San Diego, CA) CCD 4915 camera and a Sony SVO-95000MD video recorder. A more thorough discussion of the apparatus can be found in previous publications (Chalmers et al., 1999a, 1999b, 1999c).

CTV Analysis

Analog VCR images from videotapes were converted into 624 \times 450 pixel images in which each pixel was assigned a gray level ranging from 0 (black) to 255 (white or brightest) with a μ Tech image board (Mutech Corp., Billerica, MA) and M-Vision 1000 Sequence Software (Mutech Corp., Billerica, MA). This software allows the user to adjust gain and offset settings to improve image quality before recording and saving images from the videotape or directly from the camera, and converting them into pixel (digital) form. The software also allows the user to choose how many total number of frames, or images, to save as well as how many frames to skip before saving the next image. This frame-skipping feature is an important tool that can sometimes significantly reduce noise in the final velocity data. A more complete discussion of the accuracy of CTV can be found in Nakamura et al. (2001).

Execution of proprietary Borland C++ programs that identify the moving particles and calculate their velocities, allows the velocities for each cell/microbead to be converted into magnetophoretic mobilities using mathematical models. More details are provided in separate publications (Chalmers et al., 1999a, 1999b, 1999c).

RESULTS

Fluorescent Intensities of CD4+ Cells

Figure 3 is a semi-log histogram depicting the fluorescence intensities of the anti-CD4-labeled PBMNs. This plot illustrates the low level of CD4 expression on monocytes as the "dim" peak, compared with the CD4 positive lymphocyte population, the "bright" peak. The cell population of each peak was verified by gating (side

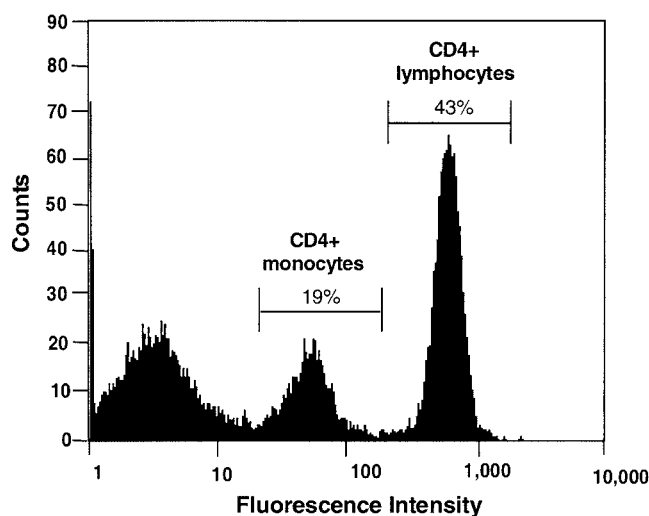


Figure 3. Semi-log histogram showing the fluorescence intensities of peripheral blood mononuclear cells. The brightest cells are the CD4+ T-lymphocytes and the dimly fluorescent cells are the monocytes.

scatter vs. forward scatter) for the larger mononuclear cells only, which effectively eliminated the “bright” and the nonfluorescent peak (data not shown). Likewise, gating on the smaller-sized lymphocyte population eliminates the “dim” monocyte peak (data not shown). The results shown in Figure 3 are verified by independent results reporting that monocytes express lower numbers of CD4 antigens, ABC = 17,000, than CD4+ T-cells, ABC = 47,000 (Bikoue et al., 1996).

Monocyte Depletion

Because a heterogeneous population of cells that are expressing multiple levels of CD4 molecules would add variability to the magnetophoretic mobility measurements, the monocyte cell population was depleted from the leukocyte source prior to immunomagnetic labeling. Monocyte depletion was verified using a Coulter Multisizer II instrument for cell-size distribution analysis. Figure 4a,b depicts the cell-size distribution of normal

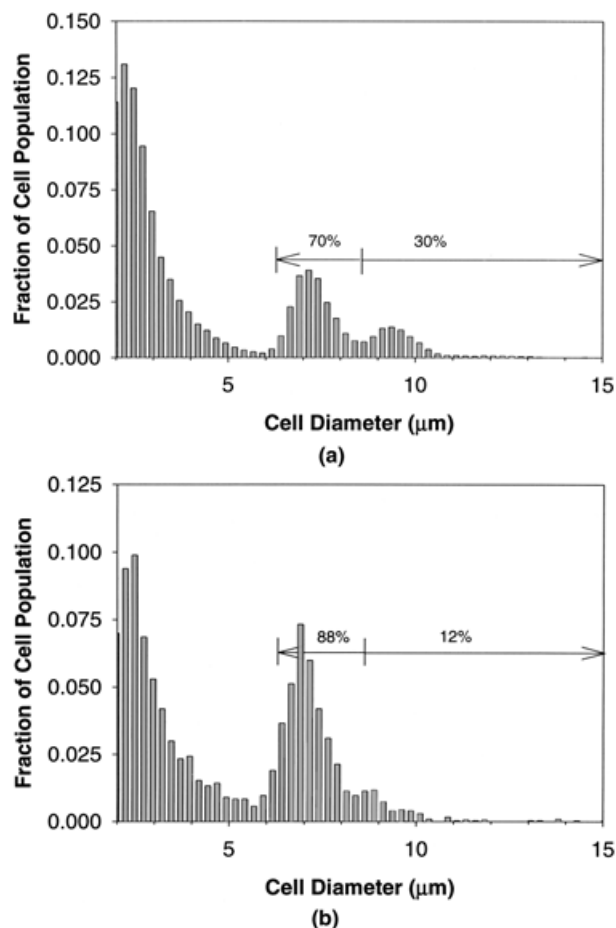


Figure 4. (a) Cell-size histogram of the white blood cell population separated on a Ficoll cushion. The largest cells represent the monocyte cell population. (b) Cell-size histogram of the white blood cell population separated on a Ficoll cushion after monocyte depletion. Note the decrease in the large cell fraction as compared with panel (a).

blood cells used in this study before and after monocyte depletion, respectively. The lymphocyte size range fell between 6.1 microns and 8.3 microns while the monocytes size range fell between 8.4 microns and 15 microns. The monocyte depletion process resulted in a reduction of the larger cell peak, from approximately 30% down to 12% of the white blood cell population. The residual red blood cell population also decreased during the monocyte depletion procedure.

IgG Blocking

A control study was also conducted on the use of human IgG blocker to block the nonspecific binding of the secondary antibody. The linear histograms shown in Figure 5 depict the magnetophoretic mobilities of cells from this control study. The cells were labeled with and without IgG blocking reagent, then nonspecifically using secondary anti-FITC MACS magnetic nanoparticle antibodies without any primary antibody. Note that both of these plots are centered approximately at zero velocity, although the mobilities of the nonblocked cells are slightly greater than that of the blocked cells. The mean mobility of the nonblocked cells is 4.5×10^{-6} mm³/T-A-s and the mean mobility of the blocked cells is -5.2×10^{-6} mm³/T-A-s (millimeter cubed per tesla-ampere-second). A two-sample t-procedure for comparing means indicated that the IgG blocker is significantly reducing the nonspecific binding ($P < 0.0005$, $N \approx 400$).

Magnetophoretic Mobilities of CD4+ Cells

Figures 6a, 7a, 8a, and 9a are semi-log histograms depicting magnetophoretic mobility results of the immunomagnetically labeled lymphocytes using the four different antibody-labeling schemes portrayed in Figure

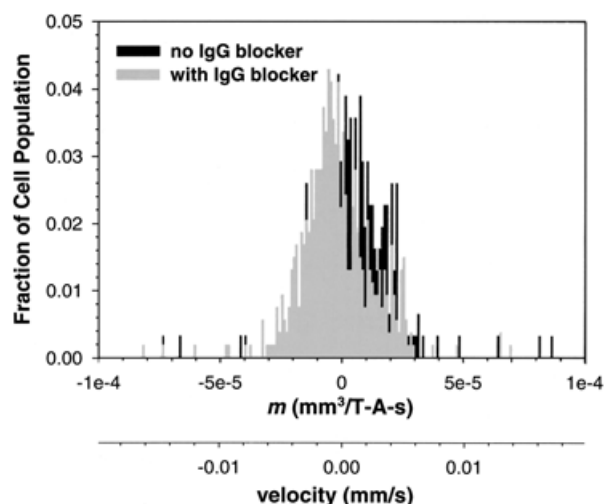
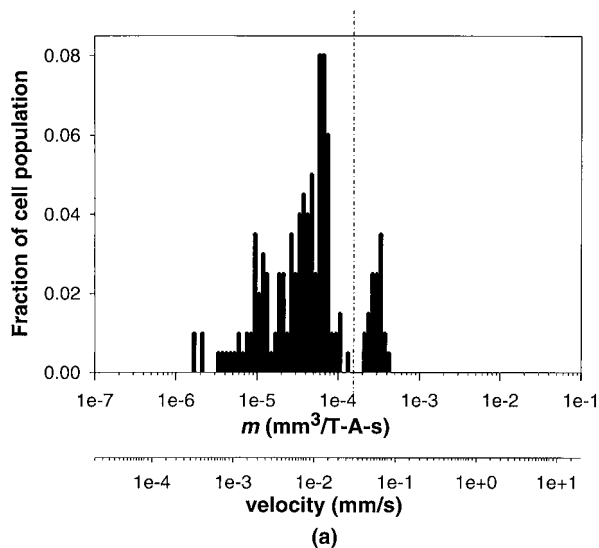
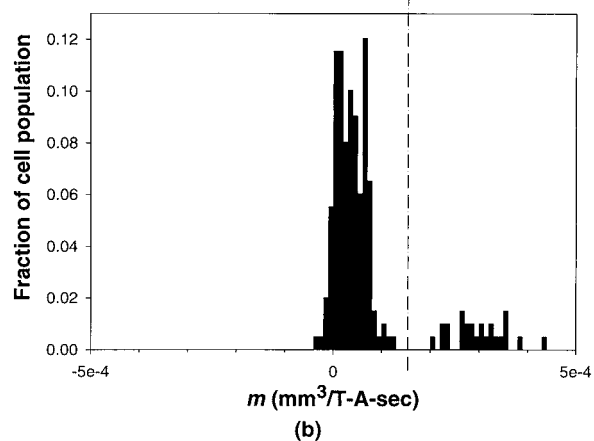


Figure 5. Semi-log histogram of the mobilities of the cells labeled with an irrelevant antibody (with and without IgG blocking reagent).



(a)

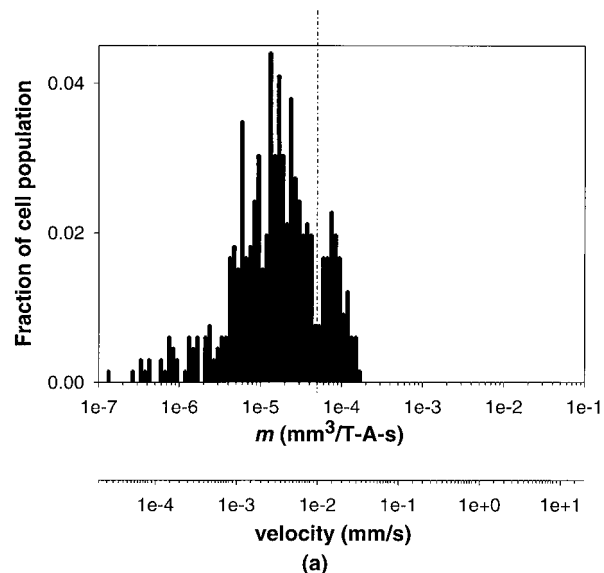


(b)

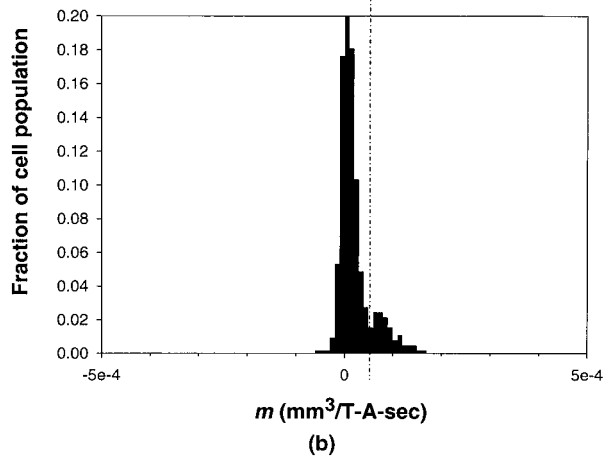
Figure 6. (a) Semi-log histogram of the magnetophoretic mobilities (and corresponding velocities) of the cells labeled with anti-CD4 FITC and anti-FITC MACS magnetic nanoparticles (labeling scheme 1). (b) Linear histogram of the magnetophoretic mobilities of the cells labeled with anti-CD4 FITC and anti-FITC MACS magnetic nanoparticle antibody, $N_{total} = 200$.

la-d. Figures 6b, 7b, 8b, and 9b are the corresponding linear histograms. The distinction between the negative and positively labeled cells is visually observed as the “valley” between the two mobility peaks. Note that for the labeling scheme which produced the highest mobilities as seen in Figure 6a,b the two peaks are clearly separated, unlike the labeling scheme which produced the lowest mobilities as seen in Figure 9a,b.

The mobility histograms in Figure 6a,b consist of cells immunomagnetically labeled with mouse anti-CD4 FITC primary antibody, then mouse anti-FITC MACS magnetic nanoparticle secondary antibody following antibody labeling scheme 1 as presented in Figure 1a. The mean mobility values were calculated using data within the positive peak area only. The mean mobility of the positive peak in Figure 6a is $m_{1,2} = 3.0 \times 10^{-4} \pm 2.2 \times 10^{-5} \text{ mm}^3/\text{T-A-s}$ (margin of error, 95% confidence limit, $N = 26$).



(a)



(b)

Figure 7. (a) Semi-log histogram of the magnetophoretic mobilities (and corresponding velocities) of the cells labeled with anti-CD4 MACS magnetic nanoparticle antibody (labeling scheme 2). (b) Linear histogram of the magnetophoretic mobilities of the cells labeled with anti-CD4 MACS magnetic nanoparticle antibody, $N_{total} = 658$.

The cells in Figure 7a,b were immunomagnetically labeled directly with mouse anti-CD4 MACS magnetic nanoparticle antibodies following the antibody-labeling scheme 2 presented in Figure 1b. The mean mobility of the positive peak in Figure 7a is $m_{1D} = 8.8 \times 10^{-5} \pm 5.5 \times 10^{-6} \text{ mm}^3/\text{T-A-s}$ (margin of error, 95% confidence limit, $N = 89$).

The cells in Figure 8a,b were immunomagnetically labeled with mouse anti-CD4 FITC primary antibody, then rat anti-mouse MACS magnetic nanoparticle secondary antibody following the antibody-labeling scheme 3 presented in Figure 1c. The mean mobility of the positive peak in Figure 8a is $m_{1,2m} = 8.6 \times 10^{-5} \pm 4.6 \times 10^{-6} \text{ mm}^3/\text{T-A-s}$ (margin of error, 95% confidence limit, $N = 75$).

The cells in Figure 9a,b were immunomagnetically labeled with equal volumes of mouse anti-CD4 FITC

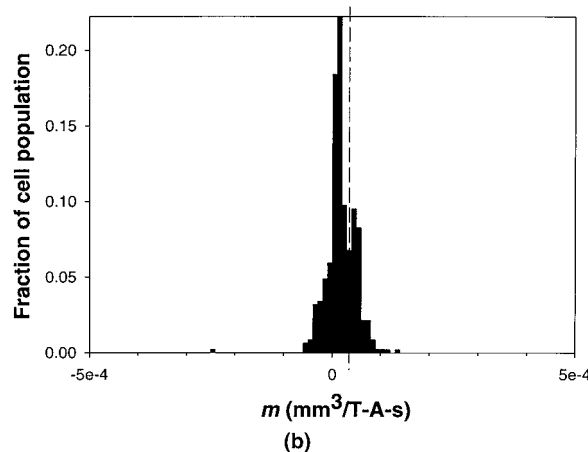
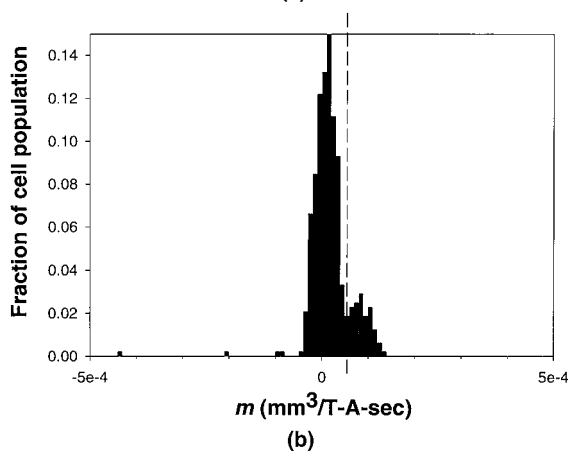
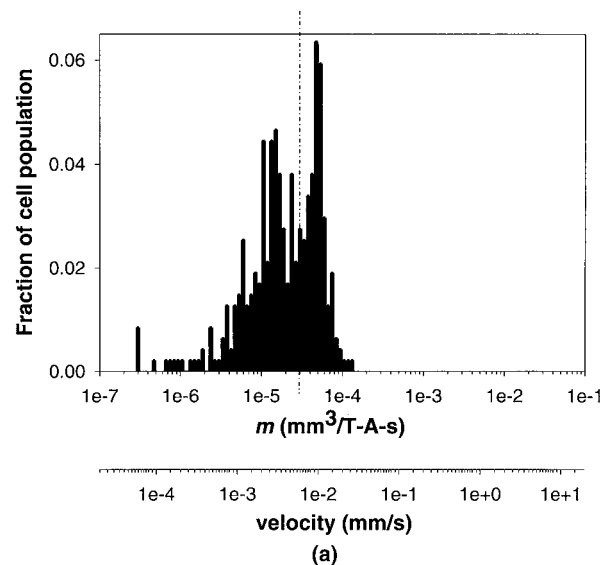
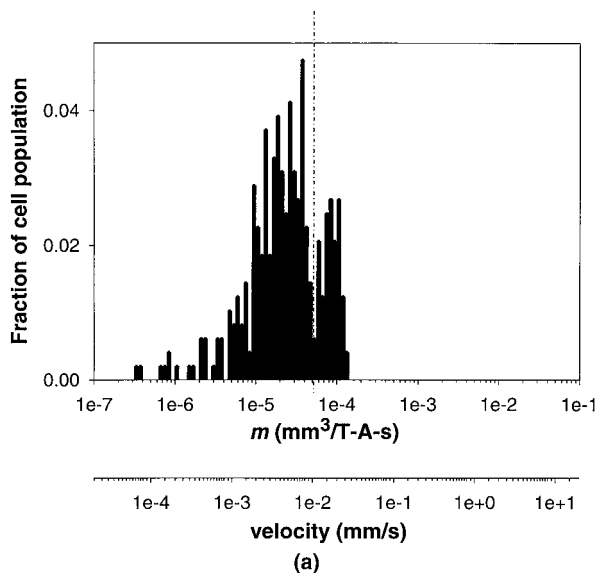


Figure 8. (a) Semi-log histogram of the magnetophoretic mobilities (and corresponding velocities) of the cells labeled with mouse anti-CD4 FITC antibody and anti-mouse MACS magnetic nanoparticle antibody (labeling scheme 4). (b) Linear histogram of the magnetophoretic mobilities of the cells labeled with mouse anti-CD4 FITC antibody and anti-mouse MACS magnetic nanoparticle antibody, $N_{total} = 484$.

Figure 9. (a) Semi-log histogram of the magnetophoretic mobilities (and corresponding velocities) of the cells labeled with FITC conjugated and unconjugated anti-CD4 antibodies and anti-FITC MACS magnetic nanoparticle antibody (labeling scheme 4). (b) Linear histogram of the magnetophoretic mobilities of the cells labeled with FITC conjugated and unconjugated anti-CD4 antibodies and anti-FITC MACS magnetic nanoparticle antibody, $N_{total} = 472$.

primary antibody and mouse anti-CD4 Pure (unconjugated) primary antibody, then mouse anti-FITC MACS magnetic nanoparticle secondary antibody following the antibody-labeling scheme 4 presented in Figure 1d. The mean mobility of the positive peak in Figure 9a is $m_{1,2\phi} = 5.0 \times 10^{-5} \pm 2.7 \times 10^{-6} \text{ mm}^3/\text{T-A-s}$ (margin of error, 95% confidence limit, $N = 154$).

Analysis of Magnetophoretic Mobility Amplification

The theory described above was applied to the measured magnetophoretic mobility data to calculate the antibody-binding amplification, $\Psi_{1,2f}$, and $\Psi_{1,2m}$, resulting from secondary antibodies binding to multiple sites on each primary antibody. By substituting the experimental mobility data from cells labeled according to scheme 1

and scheme 2 into Equation (9), we obtained $\Psi_{1,2f} = 3.4 \pm 0.33$ (margin of error, 95% confidence limit). This indicates that an average of 3.4 anti-FITC MACS magnetic nanoparticle secondary antibodies bind to every one primary CD4 FITC antibody. Likewise, from Equation (11) and mobility data from cells labeled according to schemes 2 and 3, we obtained $\Psi_{1,2m} = 0.98 \pm 0.081$ (margin of error, 95% confidence limit). This indicates that approximately 1 anti-mouse MACS magnetic nanoparticle secondary antibody binds to each primary CD4 FITC mouse antibody.

Calculation of the Fraction of Competing Primary Antibody

The fourth antibody-labeling scheme incorporated a 50:50 by volume mixture of FITC-conjugated and

unconjugated (pure) primary CD4 antibodies. The unconjugated antibody was added to compete with the mouse anti-CD4 FITC-conjugated antibodies. Because fewer FITC conjugated antibodies would be binding to the cells, the total number of sites available for the secondary antibody to bind would also decrease. The proportion of FITC-conjugated antibody to unconjugated antibody can be estimated using information provided from the vendor. The provided antibody concentrations were: 3 $\mu\text{g}/\text{mL}$ for the FITC-conjugated reagent and 25 $\mu\text{g}/\text{mL}$ for the unconjugated CD4 antibodies. Based on this information, and the fact that we used equal volumes of antibody reagent, we estimate that only 11% of the antibodies in the mixture will have the FITC molecules conjugated to them, thus providing binding sites for the secondary antibody.

From Equation (14) and mobility data from cells labeled according to the protocol in scheme 4 and scheme 1, we obtained a value for the fraction of FITC sites now available, $\phi = 0.17 \pm 0.015$ (margin of error, 95% confidence limit) as compared with the number available in labeling scheme 1. This number indicates that the fraction of binding sites on the primary antibody for secondary antibody binding is only 17% of the total number of sites available compared with when using mouse anti-CD4 FITC alone. This fraction also provides information about the relative concentration of FITC-conjugated and unconjugated (pure) CD4 antibodies in the 50/50 v/v mixture; 17% of the antibodies are FITC-conjugated anti-CD4 antibodies and 83% are unconjugated anti-CD4 antibodies. The calculated fraction of antibodies in the mixture that have been FITC-conjugated, 17%, is only slightly greater than the estimated value of 11% from the vendor information.

The calculated value for ϕ may also be obtained using an independent method of analysis, FCM. In FCM analysis, the fluorescence intensity (FI) of an immunofluorescently labeled cell or microbead is proportional to the number of FITC molecules bound to that cell or microbead. Remembering that n_{2f} represents the number of FITC molecules bound to a cell or microbead, we see that the FI of the two immunofluorescently labeled populations may also be used to obtain the fraction of FITC molecules in the antibody mixture:

$$\frac{FI_{2\phi}}{FI_{2f}} = \phi \quad (15)$$

Quantum Simply Cellular calibration microbeads, commonly used in quantitative flow cytometry, were employed to check the validity of the above results. These microbeads were immunofluorescently labeled with the same 50/50 v/v of FITC-conjugated and unconjugated CD4 primary antibodies using the same reagent vials as the reagent vials used to label CD4+ cells following the labeling protocol in scheme 4.

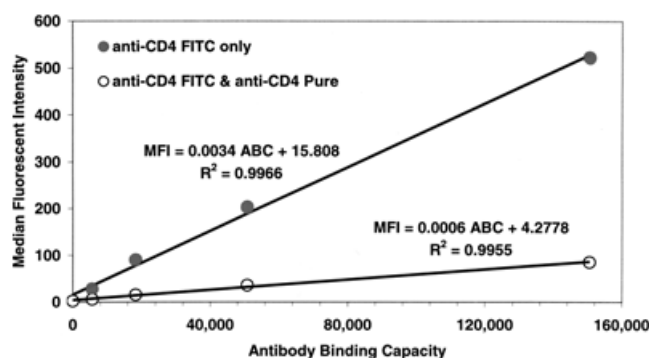


Figure 10. Linear plot of the median cellular fluorescence intensity vs. the corresponding antibody-binding capacity of Quantum Simply Cellular calibration microbeads labeled with either FITC conjugated anti-CD4 antibody and anti-FITC MACS magnetic nanoparticle antibody (closed circles), or a mixture of FITC-conjugated and unconjugated anti-CD4 antibodies and anti-FITC MACS magnetic nanoparticle antibody (open circles).

The median fluorescence intensities for each immunofluorescently labeled microbead population were plotted against that microbead's antibody-binding capacity (Fig. 10). The percentage of FITC-conjugated CD4 antibodies vs. unconjugated CD4 antibodies is obtained from a ratio of the median fluorescent intensities of the microbeads. Specifically, the median fluorescence intensity of the microbeads labeled with the mixture of FITC-conjugated and unconjugated antibodies is divided by the median fluorescence intensity of microbeads labeled with the FITC-conjugated antibody only. This was done with each for the QSC calibration microbead populations, obtaining five values for ϕ , and once for the overall linear regression slope of the two bead suspensions. In remarkable agreement with the results from the mobility measurements from antibody labeling protocol scheme 4 ($\phi = 0.17 \pm 0.015$), these FI measurements from flow cytometry also report an average value of $\phi = 0.17 \pm 0.02$ (standard deviation).

Magnetophoretic Mobilities of Magnetic Microspheres

In the histograms depicted in Figures 6–9, note that the average mobility of the negative cells is increasing with increasing average mobility of the positive (magnetized) cells. This is most clearly evident by looking closely at the line drawn in each figure separating the two peaks. The separation line is located at $m = 3 \times 10^{-5} \text{ mm}^3/\text{T-A-s}$ for the least mobile cells in Figure 9a. This separation line increases to $m = 5 \times 10^{-5} \text{ mm}^3/\text{T-A-s}$ in Figure 7a and Figure 8a, and increases again to $m = 1.5 \times 10^{-4} \text{ mm}^3/\text{T-A-s}$ for the most mobile cells in Figure 6a. This puzzling phenomenon is also consistent with the following observations from CTV analysis.

Mobility measurements of both nonmagnetic and magnetite/maghemite-coated magnetic polymeric micro-

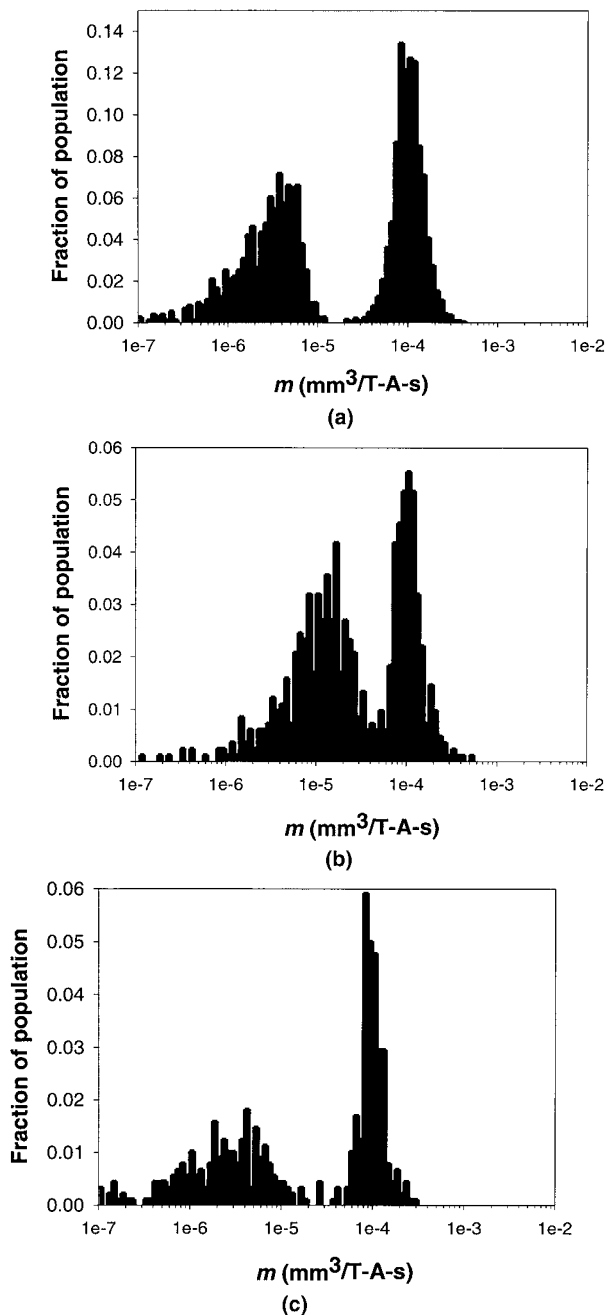


Figure 11. (a) Semi-log histogram of the magnetophoretic mobilities of magnetic (right peak) and nonmagnetic (left peak) polymeric microspheres. The microspheres in this plot were analyzed separately as pure populations. (b) Semi-log histogram of the magnetophoretic mobilities of magnetic (right peak) and nonmagnetic (left peak) polymeric microspheres. The microspheres in this plot were mixed together in equal amounts to give a final concentration of 2 million microspheres per milliliter prior to analysis. Note that these peaks are not as well separated as in panel (a). (c) Semi-log histogram of the magnetophoretic mobilities of magnetic (right peak) and nonmagnetic (left peak) polymeric microspheres. The microspheres in this plot were mixed together in equal amounts to give a final concentration of 0.5 million microspheres per milliliter prior to analysis. Note that these peaks are as well separated as in panel (a).

spheres were analyzed on our CTV system. Figure 11a displays the mobilities of these two magnetic and nonmagnetic microsphere populations. In this figure, the two populations were analyzed individually as pure populations. Figure 11b displays the mobilities of the nonmagnetic microspheres and the magnetic microspheres mixed in the same sample and analyzed together. In comparing Figure 11a,b it is apparent that the mobility of the nonmagnetic microspheres (left peak) increases from a mean mobility of $m = 2.3 \times 10^{-6}$ to $m = 1.1 \times 10^{-5} \text{ mm}^3/\text{T-A-s}$ when mixed with magnetic microspheres of higher mobility, while the mobility of the magnetic microspheres (right peak) is not affected by the presence of the nonmagnetic microspheres and remains at a mean mobility of $m = 1.1 \times 10^{-4} \text{ mm}^3/\text{T-A-s}$. In Figure 11c, the same sample of mixed magnetic and nonmagnetic beads were analyzed at a lower concentration 0.5 million beads per milliliter. By comparison, the sample concentration in Figure 11b was 2 million beads per milliliter of buffer solution. At the lower microsphere concentration, the mobilities of the nonmagnetic microsphere population do not appear to exhibit a shift towards higher mobilities as observed in the higher concentration sample.

DISCUSSION

The work presented in this article is an investigation into secondary antibody-binding amplification, Ψ , by comparing two-step antibody-labeling protocols with a single antibody-labeling protocol. This was accomplished through measuring and comparing the magnetophoretic mobilities of CD4 positive cells, immunomagnetically labeled with a direct protocol and three different indirect protocols. An understanding of these secondary antibody-binding interactions is desired because they influence the final magnetophoretic mobility of an immunomagnetically labeled cell, and thus are very important in magnetic cell separation.

It has been shown that an average of 3.4 anti-FITC MACS magnetic nanoparticle secondary antibodies bind to each primary CD4 FITC antibody, $\Psi_{1,2f} = n_{2f} \theta_{2f} \lambda_{2f} = 3.4 \pm 0.33$. This result is slightly lower than a previously predicted value, Ψ_{calc} , for number of anti-FITC MACS magnetic nanoparticle secondary antibodies binding to each primary CD2 FITC antibody. The results from this previous study led to a value for the lumped term $\beta = n_2 \theta_2 \lambda_2 n_3 = \Psi_{calc} n_3 = 4.0$ (McCloskey et al., 2000). Typically, $n_3 = 1$ (Kantor et al., 1998), therefore $\Psi_{calc} = 4.0$.

One possible reason for the discrepancy between $\Psi_{1,2f} = 3.4$ and $\Psi_{calc} = 4.0$ is that the magnetic nanoparticles are physically limited from binding to CD4 cells. (Gee et al., 1991; McCloskey et al., 2000) Steric hindrance would act by lowering the number of magnetic nanoparticles that can bind per available binding site, thus

lower the value θ_2 [Eq. (3)]. It has been calculated that for antibodies exhibiting this level of amplification, steric hindrance effects will begin above approximately 30,000 ABC (McCloskey et al., 2000). Because it has also been well documented that T-cell associated CD4 molecules exhibit approximately 47,000 ABC (Bikoue et al., 1996; Davis et al., 1998; Poncelet, 1991), we would expect to see some amount of steric hindrance on the CD4 immunomagnetically labeled cells. We conclude that the lower value of $\Psi_{1,2f} = 3.4$ compared with $\Psi_{calc} = 4.0$ for the immunomagnetically labeled CD4 positive cells is due to steric hindrance limiting the binding of the magnetic nanoparticles to the cellular surface.

For the cells labeled according to the protocol in scheme 3, the secondary antibody-binding amplification was calculated to be $\Psi_{1,2m} = 0.98 \pm 0.081$. In other words, there was approximately one anti-mouse MACS magnetic nanoparticle secondary antibody binding to each primary CD4 FITC mouse antibody on the CD4 positive lymphocytes. At this low level of antibody binding, the steric hindrance described above would be negligible. The current methodology does not allow one to distinguish between possible secondary antibody-binding mechanisms. One possible binding mechanism involves only one IgG1 mouse binding site per anti-mouse MACS magnetic nanoparticle antibody with monovalent antibody binding, in which case $n_{2m} = 1$, $\theta_{2m} = 0.98$, and $\lambda_{2m} = 1$. The second binding mechanism involves two mouse binding sites per anti-mouse MACS magnetic nanoparticle antibody with bivalent antibody binding, meaning that each rat anti-mouse antibody binds two mouse antigen sites on each primary antibody, in which case $n_{2m} = 2$, $\theta_{2m} = 0.98$, and $\lambda_{2m} = 1$.

From the magnetophoretic mobility data in this study (Figs. 6–9), it appears as if the mobile cells are imparting a very small mobility to the nonmobile cells and that this mobility is proportional to the mobility of the mobile cells. In addition, the magnetophoretic mobility results using magnetic microspheres depicted in Figure 11a–c verifies this phenomenon and indicates that this effect on the nonmobile microspheres is concentration dependent. At lower concentrations, the mobilities of the microsphere populations do not appear to exhibit the same shift towards higher mobilities as observed in the higher concentration sample. Our labs are continuing to investigate the cause of these shifting mobilities of the nonmagnetic cell and microsphere populations.

The results shown in Figure 11a–c, using magnetite-doped polymer microspheres, are important in analysis of CD4 cellular mobilities because these results immediately eliminate two other factors as possibly responsible for the mobility increase of the negative cell population with increasing mobility of the CD4 positive cell population. These two other factors include nonspecific antibody binding or monocyte contamination. Also, because this phenomenon of shifting mobilities does not appear to affect the positive, faster moving cell population, the

mobility calculations for each of our antibody-labeling schemes are also expected to be unaffected.

The overall goal of our research is to develop magnetic separation devices and techniques. The ability to impart magnetophoretic mobility on a target cell is a crucial part of any magnetic separation technique. Mathematical equations have been proposed which model the magnetic nanoparticle antibody binding mechanisms used to impart this magnetophoretic mobility on a target cell (McCloskey et al., 2000). In addition, the primary antibody binding parameters, $n_1\theta_1\lambda_1$, or antibody binding capacity (ABC), have been investigated and quantitated (McCloskey et al., 2000; 2001). The work presented herewith continues examination of the antibody-binding mechanisms to study the amplification of magnetophoretic mobility due to secondary antibody-binding parameters, $\Psi = n_2\theta_2\lambda_2$. Combined, these three publications provide a significant amount of information about the antibody-binding mechanisms involved in immunomagnetically labeling a target cell for magnetic separation.

This work has been supported by grants from the National Science Foundation (BCS-9258004, BES-9731059 to J.J.C.) and the National Cancer Institute (R01 CA62349 to M.Z. and R33 CA81662-01 to J.J.C.).

NOMENCLATURE

ABC	antibody-binding capacity	
B	magnetic flux density	(tesla)
D_c	diameter of the cell or microbead	(m)
$F_b = kS_m$	magnetic force acting on one paramagnetic nanoparticle	(kg-m/s ²)
F_{bou}	buoyancy force	(kg-m/s ²)
F_d	drag force	(kg-m/s ²)
F_g	gravitational force	(kg-m/s ²)
F_m	magnetic force	(kg-m/s ²)
f	friction coefficient	(kg/s)
$k = \Delta\chi V_m$	constant representing the magnetic property of a single magnetic nanoparticle	
m	magnetophoretic mobility	(mm ³ /T-A-s)
n_{ns}	number of non-specific binding sites per cell	
n_s	number of specific antigen molecule binding sites per cell	
n_1	number of antigen-binding sites per cell	
n_2	number of binding sites on the primary antibody recognized by the secondary antibody	
n_3	number of magnetic nanoparticles conjugated to the antibody	
$S_m = \nabla B^2/2\mu_0$	magnetophoretic driving force	(tesla-ampere/mm ²)
V_m	volume of paramagnetic material per paramagnetic nanoparticle	(m ³)
v_c	velocity of moving cell or microbead	(m/s)
β	number of magnetic nanoparticles bound to each primary antibody	
χ_b	magnetic susceptibility of the magnetic material	(SI units)
χ_f	magnetic susceptibility of the fluid	(SI units)
$\Delta\chi$	difference between χ_b and χ_f	(SI units)
ϕ	fraction of binding sites available due to mixing FITC-conjugated antibody reagents with unconjugated antibodies	

η	viscosity of the suspension fluid	(kg/m-s)
λ_1	valence of primary antibody binding	
λ_2	valence of secondary antibody binding	
μ_0	magnetic permeability of free space	(tesla-m/ampere)
θ_1	fraction of antigen site on the particle surface bound by primary antibody	
θ_2	fraction of sites on the primary antibody bound by the secondary antibody	
Ψ	secondary antibody binding amplification due to secondary antibodies binding to multiple sites on the primary antibody	

References

- Asahara T, Murohara T, Sulliyana A, Silver M, van der Zee R, Li T, Witzenschnitzer B, Schatteman G, Isner JM. 1997. Isolation of putative progenitor endothelial cells for angiogenesis. *Science* 275:964-967.
- Bikoune A, George F, Poncelet P, Mutin M, Janossy G, Sampol J. 1996. Quantitative analysis of leukocyte membrane antigen expression: Normal adult values. *Cytometry* 26:137-147.
- Chalmers J, Zborowski M, Sun L, Moore L. 1998. Flow through immunomagnetic cell separation. *Biotechnol Progr* 14:141-148.
- Chalmers J, Haam S, Zhao Y, McCloskey K, Moore L, Zborowski M. 1999a. Quantification of cellular properties from external fields and resulting induced velocity: Magnetic susceptibility. *Biotechnol Bioeng* 64:519-526.
- Chalmers J, Haam S, Zhao Y, McCloskey K, Moore L, Zborowski M, Williams PS. 1999b. Quantification of cellular properties from external fields and resulting induced velocity: Cellular hydrodynamic diameter. *Biotechnol Bioeng* 64:509-518.
- Chalmers JJ, Zhao Y, Nakamura M, Melnik K, Lasky L, Moore L, Zborowski M, Williams PS. 1999c. An instrument to determine the magnetophoretic mobility of labeled, biological cells and paramagnetic particles. *J Magn Magn Mater* 194:231-241.
- Davis K, Abrams B, Iyer S, Hoffman R, Bishop J. 1998. Determination of CD4 antigen density on cells: Role of antibody valency, avidity, clones, and conjugation. *Cytometry* 33:197-205.
- de Wynter E, Coutinho L, Pei X, Marsh J, Hows J, Luft T, Testa N. 1995. Comparison of purity and enrichment of CD34+ cells from bone marrow, umbilical cord and peripheral blood (primed for apheresis) using five separation systems. *Stem Cells* 13:524-532.
- Gee A, Mansour V, Weiler M. 1991. Effects of target antigen density on the separation efficacy of immunomagnetic cell separation. *J Immunol Meth* 142:127-136.
- Handgretinger R, Lang P, Schumm M, Taylor G, Neu S, Kosielnak E, Niethammer D, Klingebiel T. 1998. Isolation of transplantation of autologous peripheral CD34+ progenitor cells highly purified by magnetic-activated cell sorting. *Bone Marrow Transpl* 21:987-993.
- Kantor AB, Gibbons I, Miltenyi S, Schmitz J. 1998. Magnetic cell sorting with colloidal superparamagnetic particles. In: Recktenwald D, Radbruch A, editors. *Cell Separation Methods and Applications*. New York: Marcel Dekker, Inc. p. 153-173.
- Margel S, Gura S, Bamnolker H, Nitzan B, Tannenbaum T, Bar-Toov B, Hinz M, Seliger H. 1997. Synthesis, characterization, and use of new solid and hollow, magnetic and non-magnetic, organic-inorganic monodispersed hybrid microspheres. In: Haefeli U, Schuett W, Teller J, Zborowski M, editors. *Scientific and clinical applications of magnetic carriers*. New York: Plenum Press. p. 37-51.
- McCloskey KE, Chalmers J, Zborowski M. 2000. Magnetophoretic mobilities correlate to antibody binding capacities. *Cytometry* 40:307-315. Erratum: 2000. *Cytometry* 41:150.
- McCloskey KE, Chalmers J, Zborowski M. 2001. Measurement of CD2 expression levels of IFN- α treated fibrosarcomas using cell tracking velocimetry. *Cytometry* 44:137-147.
- Moore LR, Zborowski M, Sun L, Chalmers JJ. 1998. Lymphocyte fractionation using immunomagnetic colloid and a dipole magnet flow cell sorter. *J Biochem Biophys Meth* 37:11-33.
- Moore LR, Zborowski M, Nakamura M, McCloskey K, Gura S, Zuberi M, Margel S, Chalmers JJ. 2000. The use of magnetite-doped polymeric microspheres in calibrating cell tracking velocimetry. *J Biochem Biophys Meth* 44:115-130.
- Nakamura M, Lasky L, Zborowski M, Chalmers JJ. 2001. Theoretical and experimental analysis of the accuracy and reproducibility of cell tracking velocimetry. *Experiments in Fluids* 30:371-380.
- Poncelet P, Poinas G, Corbeau P, Devaux C, Tubiana N, Muloko N, Tamalet C, Chermann J, Kourilsky F, Sampol J. 1991. Surface CD4 density remains constant on lymphocytes of HIV-infected patients in the progression of disease. *Res Immunol* 142:291-298.
- Racila E, Euhus D, Weiss A, Rao C, McConnel J, Terstappen L, Uhr J. 1998. Detection and characterization of carcinoma cells in the blood. *Proc Natl Acad Sci USA* 95:4589-4594.
- Reddy S, Moore LR, Sun L, Zborowski M, Chalmers JJ. 1998. Determination of the magnetic susceptibility of labeled particles by video imaging. *Chem Eng Sci* 51:947-956.
- Schwartz A, Fernández-Repollet E. 1994. Standardization for flow cytometry. In: *Methods in Cell Biology*, vol. 42. San Diego: Academic Press, Inc. p. 605-626.
- Sun L, Zborowski M, Moore LR, Chalmers JJ. 1998. Continuous, flow-through immunomagnetic cell sorting in a quadrupole field. *Cytometry* 33:469-475.
- Williams PS, Zborowski M, Chalmers JJ. 1999. Flow rate optimization for the quadrupole magnetic cell sorter. *Anal Chem* 71:3799-3807.
- Zagursky R, Sharp D, Solomon K, Schwartz A. 1995. Quantitation of cellular receptors by a new immunocytochemical flow cytometry technique. *Biotechniques* 18:504-509.
- Zborowski M, Sun L, Moore LR, Williams PS, Chalmers JJ. 1999. Continuous cell separation using novel magnetic quadrupole flow sorter. *J Magn Magn Mater* 194:224-230.